Journal of Magnetism and Magnetic Materials 323 (2011) 1950–1953

Contents lists available at ScienceDirect

Journal of Magnetism and Magnetic Materials

journal homepage: www.elsevier.com/locate/jmmm

Magnetic properties of electroless-deposited Ni and Ni–NiO core–shell nano-arrays

Chih-Chieh Lo [a], Chun-Chao Huang [a], Chien-Min Liu [a], Chih Chen [a], Chang-Yang Kuo [b], Hong-Ji Lin [b], Yuan-Chieh Tseng [a,*]

[a] Department of Materials Science and Engineering, National Chiao-Tung University, Hsin-chu 30010, Taiwan
[b] National Synchrotron Radiation Research Center, Hsin-chu 30077, Taiwan

ARTICLE INFO

Article history:
Received 30 November 2010
Received in revised form
9 February 2011
Available online 1 March 2011

Keywords:
Electroless deposition
Nano-array
Core-shell
X-ray magnetic circular dichroism
Anodic aluminum oxide

ABSTRACT

Ni and Ni–NiO core–shell nano-arrays were fabricated by means of electroless deposition, where the latter was covered by a NiO shell of ~10 nm by annealing the former at 350 °C for 30 min in an atmospheric condition. HRTEM showed that the NiO shell was developed at the expense of Ni at the array's surface. Ferromagnetic ordering of the Ni–NiO arrays was found to be suppressed compared with those of the less oxidized reference Ni arrays. This is attributed to the screening effect of the NiO shell, and weak ferromagnetism of inner Ni arrays resulted from the development of the NiO. X-ray absorption spectrum reveals that the reference Ni is partially oxidized. Also, X-ray magnetic circular dichroism suggests that the magnetic suppression of the Ni–NiO arrays is associated with a reduced spin moment.

1. Introduction

Materials that exhibit both antiferromagnetism (AFM) and ferromagnetism (FM) in close proximity are interesting for understanding both the fundamental magnetic interactions and their potential application in new electronic devices.

Examples can be found in the exchange bias at the AFM–FM interface, spin-transport across the interface, or spin-dependent magnetoresistance in spin-valve structures [1–4]. The overall magnetic properties may vary significantly when the two magnetisms coexist, depending on their fractional volumes, their anisotropies, their responses to the applied field, the environmental temperature, and other factors [5–9]. Recent advances in nanotechnology have turned the focus on the AFM–FM interface into a low dimensional framework, where the magnetic interactions between the two dissimilar magnets were found to become more vigorous due to large AFM–FM contact area [10,11]. In this paper, we investigate the magnetic properties of Ni and Ni–NiO core-shell nano-arrays, aimed at understanding how the NiO shell influences the entire array. The results demonstrate that though the NiO is only ~10 nm, its AFM strength can screen the inner Ni-FM and cause the magnetic properties of entire array to differ greatly from those of a reference Ni nano-array.

2. Experimental

Highly oriented Ni nano-arrays of diameter 70 nm and length 320 nm were fabricated directly onto Si substrates by electroless plating using an anodic aluminum oxide (AAO) template [12]. Prior to the electroless-deposition process, the AAO–Si sample was sensitized and activated by a $SnCl_2$/HCl solution (40 g/L $SnCl_2$ + 3 ml/L HCl) and a $PdCl_2$/HCl solution (0.15 g/L $PdCl_2$ + 3 ml/L HCl). The electroless-plating solution was composed of $NiSO_4$ as the main Ni source, NaH_2PO_2 as the reducing agent, $Na_2C_4H_4O_4$ as the stabilizing agent, and $Pb(NO_3)_2$ as the buffer agent. The array's configuration was probed using a scanning electron microscope (SEM) operated at 15 kV. After the removal of the AAO, the Ni/Si samples were post-annealed at 350 °C for 30 min in an atmospheric condition to develop a Ni–NiO core-shell structure. Meanwhile, a set of reference Ni arrays having the same dimensions as those of the first sample were prepared. The reference Ni sample was then annealed at 350 °C for 30 min. in a vacuum condition, with the AAO present to prevent the formation of NiO. This was to ensure that the difference in the probed magnetic properties between the two samples could be completely attributed to the presence of NiO. Afterwards, high-resolution transmission electron microscopy (HRTEM) imaging was employed to probe the microstructures of the two arrays. Energy-dispersive X-ray spectroscopy (EDX) attached to the TEM was used to probe the local atomic percentages of the samples. Magnetic hysteresis (M–H) curves were collected at 30 K using a superconducting quantum interference device

* Corresponding author. Tel.: +886 3573 1898; fax: +886 3572 4727.
E-mail address: yctseng21@mail.nctu.edu.tw (Y.-C. Tseng).

0304-8853/$ - see front matter © 2011 Elsevier B.V. All rights reserved.
doi:10.1016/j.jmmm.2011.02.028

(SQUID), with a magnetic field applied along arrays' long and short axes. X-ray absorption spectroscopy (XAS) was collected over Ni L_2 and L_3 edges to probe the samples' chemical states and electronic structures that are coupled to the magnetism. Meanwhile, X-ray magnetic circular dichroism (XMCD) spectra were taken in total electron yield (TEY) mode over XAS with opposite helicities to decouple orbital (L_z) and spin (S_z) moments using the XMCD sum rules [13]. X-ray data were all taken at $T=30$ K and $H=1$ T, with both X-ray photon wave vector and magnetic field parallel to the array's long axis, at beamline 11A of the National Synchrotron Radiation Research Center (NSRRC) in Taiwan.

3. Results and discussion

Fig. 1 shows a SEM image of the Ni nano-arrays demonstrating the free-standing nature of the arrays on a Si substrate. The highly ordered nature of the nano-arrays presents potential use of perpendicular magnetic recording. Fig. 2(a) and (b) reveal the microstructures of the array's surfaces for the reference Ni and the core-shell Ni–NiO samples, respectively. Without the AAO protection, a NiO layer with a thickness of ~10 nm was developed onto the Ni array's surface upon heat treatment. NiO layers with similar thickness were seen elsewhere in the same sample, suggesting that the Ni–NiO core-shell structure is present along the entire rod. The NiO's phase was verified by selected-area-electron-diffraction (SAED) taken with a fast Fourier transformation (FFT) mode, which is shown in the inset. The observed diffraction pattern is consistent with the results of atomic percentages probed by EDX, which found the Ni and O concentrations to be 52% and 48%, respectively. Since the outer shell material was found to be composed of NiO it is reasonable to expect the AFM ordering in this region of the nano-rod. The NiO is formed at the expense of Ni, likely through a Ni-outward and O-inward diffusion mechanism [14]. The diffusion mechanism also developed a heterogeneous interface that physically separated the core and shell. This allowed the bulk of the inner Ni to behave somewhat independently of the NiO-AFM in response to the field application. On the other hand, the HRTEM demonstrated a polycrystalline structure for both the Ni–NiO and the reference Ni samples. Our previous work found that the as-deposited Ni featured a nano-crystalline structure [12], and a superparamagnetic (SM)→ferromagnetic phase transition of the arrays took place upon annealing. The conclusion was drawn that the magnetic transition is coupled to a microstructural modification that changes from nano-crystalline to polycrystalline phase [12]. This suggests that the microstructure can serve as an indicator of the magnetic ordering state and that a polycrystalline structure, regardless of its level of crystallinity, can be presumed to be in an FM state in accordance with the results shown in Figs. 2(a) and 3(a).

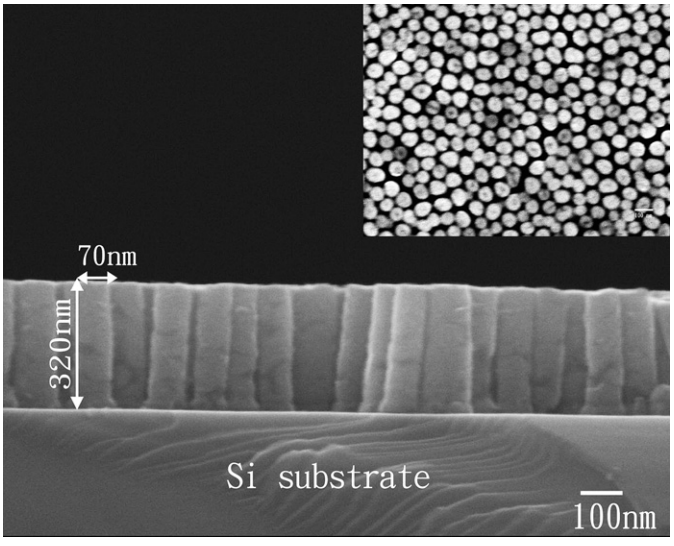

Fig. 1. SEM cross-section (main figure) and top view (inset) images of Ni nano-arrays on a Si substrate.

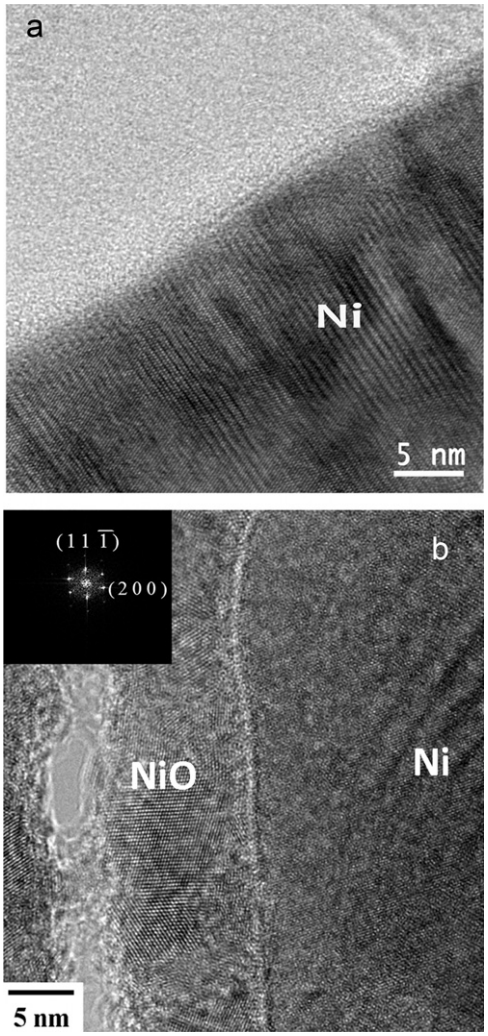

Fig. 2. HRTEM images of the surfaces of (a) Ni and (b) Ni–NiO nano-arrays. Inset of (b) shows the SAED of the NiO layer, which was taken at a fast Fourier transformation (FFT) mode.

Fig. 3 demonstrates the *M–H* curves for (a) the reference Ni and (b) the Ni–NiO samples with magnetic field applied along the array's long and short axes. Both samples display magnetic anisotropy along the long axis, while the reference Ni exhibits a more significant FM hysteresis curve than does the Ni–NiO. Since the inner Ni of the Ni–NiO sample has a polycrystalline structure, it should display FM ordering similar to the reference Ni, as shown in Fig. 3(a). However, the linear *M–H* obtained in Fig. 3(b) indicates a magnetic suppression that can be related to the presence of the NiO shell and could be attributed to two explanations. First could be the strong masking effect of the NiO-AFM upon the inner Ni as a result of the large shell coverage of the core-shell structure [15]. In particular, AFM moments are hard to cant by the field application because of the absence of FM domain walls. Besides, the AFM/FM coupling may occur across the NiO/Ni interface, which is inclined to pin the Ni-FM moments

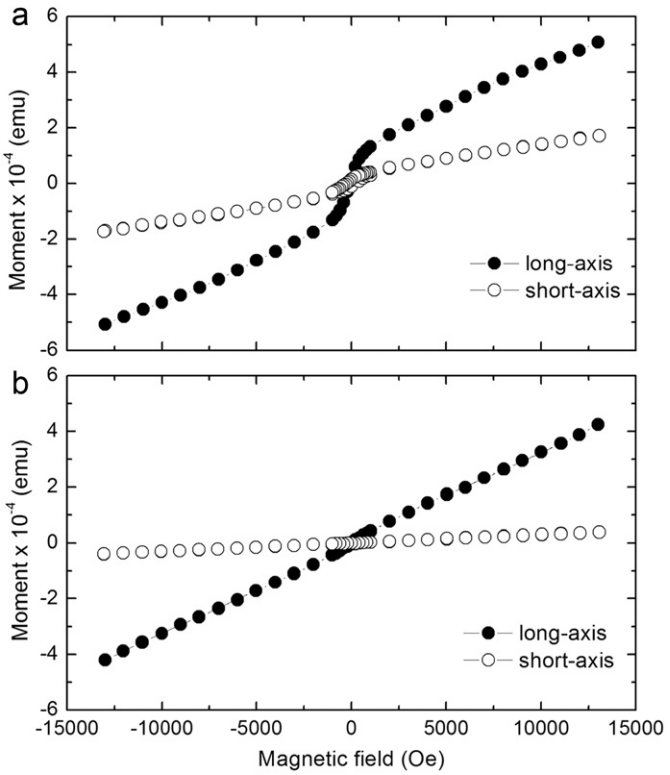

Fig. 3. *M–H* curves of the (a) Ni and (b) Ni–NiO nano-arrays, with magnetic field applied along long (filled circles) and short (open circles) axes. Data were collected at $T=30$ K, with a zero-field-cooling condition.

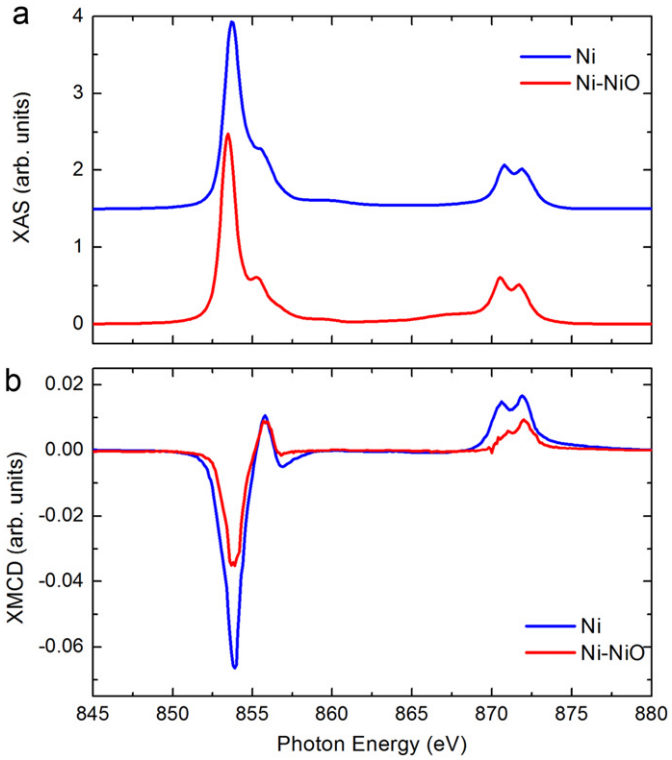

Fig. 4. (a) XAS and (b) XMCD spectra of Ni L_2, L_3 edges for the Ni (blue) and the Ni–NiO (red) nano-arrays. For (a), the absorption backgrounds have been subtracted. (For interpretation of the references to colour in this figure legend, the reader is referred to the web version of this article.)

within a few nanometers from surface to bulk. This reduces FM moments' degree of freedom in response to the applied field and results in a low magnetization.

The screening effect of the shell is further suggested by the nearly zero magnetization measured along the short axis, as shown in Fig. 3(b). This indicates a remarkable demagnetization resulting from the 10 nm NiO-AFM layer. The difference between the two samples' *M–H* curves primarily lies in low field range ($<$ 2500 Oe), where the Ni–NiO sample displays much smaller magnetization than does the reference Ni. Nevertheless the slopes of the two samples' *M–H* curves are in close proximity along the long axis, possibly because the NiO-AFM's suppression on the Ni-FM is more dominant at low field, while in higher field range ($>$2500 Oe) the Ni-FM moments are able to overcome the shell's influences and switch freely as with the absence of the NiO-AFM. Second, since the outer NiO is formed at the expense of the inner Ni, the volume fraction and FM strength of the inner Ni are expected to be somewhat less than that of the reference Ni, depending on the consumed volume. We used the HRTEM results (Fig. 2) to quantify the Ni volumes of the two samples, and correlated them with the reduced magnetization of the Ni–NiO as compared with that of the Ni sample (Fig. 3). Regardless of the AFM–FM interfacial interactions and assuming that the magnetization is proportional to the Ni volume, the reduced magnetization of the Ni–NiO sample agrees well with its reduced Ni volume when compared with the Ni sample.

We found that magnetically, the AFM and FM strengths of the Ni–NiO sample exhibit opposite dependencies on the post-annealing. The development of NiO-AFM consumes Ni-FM simultaneously, hence lowering the total magnetization of the Ni–NiO sample. Here, we believe that first and second causes are both responsible for the linear *M–H* of the Ni–NiO sample.

The XAS of the reference Ni sample shown in Fig. 4(a) features satellite peaks around the main Ni L_2 and L_3 edges, suggesting oxidation of the sample [16,17]. This is consistent with the EDX analysis, which shows the sample's oxygen atomic percentage as $\sim$15%. More obvious splittings between the satellite and the main peaks are seen in the Ni–NiO sample, meaning that the NiO phase dominates the Ni–NiO sample electronically due to the large coverage area. The oxidation of reference Ni probably took place while annealing, because the adjacent AAO may have served as an oxygen source to the Ni sample. The oxidation of Ni was not enough to form a physical layer as that of Ni–NiO, but it may explain the non-saturated magnetization at high field because of the partial NiO phase. Thus, preventing the oxidation of Ni during electroless-deposition is the key for the array's applications in perpendicular recording. Fig. 4(b) shows the XMCD signals corresponding to XAS L_2 and L_3 edges for the two samples. Sum rule results estimated from the spectra show that the L_z values for the two samples are small and within experimental error of each other (Ni and Ni–NiO have L_z values of $\sim$0.035(5) and 0.029(3) μ_B/atom, respectively). For the Ni–NiO the X-ray-probed moments are the combination of the Ni-FM and the canted NiO-AFM moments mostly at the rod's surface, considering that the TEY measurement is surface sensitive. However, the Ni–NiO sample is considered a whole unity in our sum rules interpretation. The estimates for S_z and L_z could have been affected by a poorly defined n_{3d} [13], while the L_z/S_z ratio should be independent of the concern. Our results show that Ni and Ni–NiO have $L_z/S_z=\sim$0.16 and 0.33, respectively. The smaller L_z/S_z of Ni–NiO indicates that its magnetic suppression can be correlated to, at least qualitatively, the reduction in spin moment at rod's surface contributed independently from Ni-FM and NiO-AFM.

4. Conclusion

In summary, we have investigated how the NiO shell influences the magnetic properties of Ni nano-arrays. The results

demonstrate that due to large coverage of the outer NiO and an undermined FM strength of the inner Ni, the magnetic ordering of the Ni–NiO is suppressed compared with that of the reference Ni arrays. The results of X-ray and sum rules suggest that the suppression is primarily dominated by the reduction of spin moment concomitantly given by the NiO and the Ni.

Acknowledgements

This work is supported by the National Science Council of Taiwan under Grant No. NSC 98-2112-M-009 022-MY3.

References

[1] J. Sort, V. Langlais, V. Skumryev, S. Surinach, J.S. Munoz, M.D. Baro, Phys. Rep. 422 (2005) 65.
[2] I.N. Krivorotov, H. Yan, E.D. Dahlberg, A. Stein, J. Magn. Magn. Mater. 226 (2001) 1800.
[3] Y.Y. Kuznetsova, S. Yang, L.V. Butov, T. Ostatnick, A. Kavokin, A.C. Gossard, Nano Lett. 9 (2009) 4204.
[4] C. Prados, C.Y. Ni, G.C. Hadjipanayis, J.Q. Xiao, J. Magn. Magn. Mater. 189 (1998) 25.
[5] S.W. Jung, W.I. Park, G.-C. Yi, M.Y. Kim, Adv. Mater. 15 (2003) 1358.
[6] M. Li, Y. Wang, X. Xu, Thin Solid Films 517 (2009) 5922.
[7] H. Zheng, J. Zhong, Z. Gu, W. Wang, J. Magn. Magn. Mater. 320 (2008) 565.
[8] W.H. Meiklejohn, C.P. Bean, Phys. Rev. 102 (1956) 1413.
[9] K.P. Rajeev, Thin Solid Films 505 (2006) 113.
[10] J. Nogues, J. Sort, V. Langlais, V. Skumryev, S. Surinach, J.S. Munoz, M.D. Baro, Phys. Rep. 422 (2005) 65.
[11] Y. Choi, Y.C. Tseng, D. Haskel, D.E. Brown, D. Danaher, O. Chmaissem, Appl. Phys. Lett. 93 (2008) 192.
[12] C.M. Liu, Y.C. Tseng, C. Chen, M.C. Hsu, T.Y. Hsu, Y.T. Cheng, Nanotechnology 20 (2009) 415703.
[13] C.T. Chen, Y.U. Idzerda, H.-J. Lin, N.V. Smith, G. Meigs, E. Chaban, G.H. Ho, E. Pellegrin, F. Sette, Phys. Rev. Lett. 75 (1995) 152.
[14] R. Nakamura, J.G. Lee, H. Mori, H. Nakajima, Phil. Mag. 88 (2008) 257.
[15] B.B. Nayak, S. Vitta, A.K. Nigam, D. Bahadur, Thin Solid Films 505 (2006) 109.
[16] D. Alders, L.H. Tjeng, F.C. Voogt, T. Hibma, G.A. Sawatzky, J. Vogel, M. Sacchi, S. Iacobucci, C.T. Chen, Phys. Rev. B 57 (1998) 11623.
[17] Y.Z. Zhou, J.S. Chen, B.K. Tay, J.F. Hu, G.M. Chow, T. Liu, P. Yang, Appl. Phys. Lett. 90 (2007) 043111.